



HAL
open science

The effect of compressive loading on the residual gas permeability of concrete

Md Jihad Miah, Hatem Kallel, H el ene Carr e, Pierre Pimienta, Christian La Borderie

► **To cite this version:**

Md Jihad Miah, Hatem Kallel, H el ene Carr e, Pierre Pimienta, Christian La Borderie. The effect of compressive loading on the residual gas permeability of concrete. *Construction and Building Materials*, 2019, 217, pp.12-19. 10.1016/j.conbuildmat.2019.05.057 . hal-02367586

HAL Id: hal-02367586

<https://hal.science/hal-02367586v1>

Submitted on 22 Oct 2021

HAL is a multi-disciplinary open access archive for the deposit and dissemination of scientific research documents, whether they are published or not. The documents may come from teaching and research institutions in France or abroad, or from public or private research centers.

L'archive ouverte pluridisciplinaire **HAL**, est destin ee au d ep ot et  a la diffusion de documents scientifiques de niveau recherche, publi es ou non,  emanant des  tablissements d'enseignement et de recherche fran ais ou  trangers, des laboratoires publics ou priv es.



Distributed under a Creative Commons Attribution - NonCommercial 4.0 International License

1 **The Effect of Compressive Loading on the**
2 **Residual Gas Permeability of Concrete**

3
4 **Md Jihad Miah^{1*,2,3} Hatem Kallel², H el ene Carr e²,**
5 **Pierre Pimienta¹ and Christian La Borderie²,**

6 ¹Universit  Paris Est, Centre Scientifique et Technique du B timent, 84 Avenue Jean Jaur s,
7 Champs sur Marne, 77447 Marne-la-Vall e cedex 2, France

8 ²ISA BTP-SIAME, Universit  de Pau et des Pays de l'Adour, All e du Parc Montaury,
9 64600 Anglet, France

10 ³Department of Civil Engineering, University of Asia Pacific (UAP), Dhaka-1215, Bangladesh

11 **e-mails:** jihad.miah@cstb.fr, jihad.miah@uap-bd.edu, hatem.kallel@univ-pau.fr,

12 helene.carre@univ-pau.fr, pierre.pimienta@cstb.fr, christian.laborderie@univ-pau.fr

13
14 **Abstract:** Concrete permeability is related to pore connectivity and measures the flow rate of
15 gases and liquids through the concrete under a pressure gradient. Information about concrete
16 permeability - both in ordinary environmental conditions and after the exposure to high
17 temperature - is, therefore, badly needed to better understand fluid transport in concrete, with
18 specific reference to high temperature. In fact, permeability influences concrete spalling in fire
19 by favoring pore-pressure build-ups during the heating process. In this research project, two
20 different procedures are adopted to carry out permeability tests on concrete specimens either
21 unloaded or preloaded during the heating process. The results show that concrete permeability
22 strongly depends on crack width and orientation, both are affected by the axial compression or
23 radial confinement.

* Corresponding author: Md Jihad Miah
Email: jihad.miah@cstb.fr

24

25 **Keywords:** Concrete, Temperature, Permeability, Confining pressure, Uniaxial loading.

26

27 **1 Introduction**

28 Fire spalling of concrete is a complex phenomenon, which might occur due to pressure build-up
29 in the pores and thermal and load-induced stresses (Zhukov [1], Khoury and Anderberg [2],
30 Miah et al. [3]). Miah et al. [3] showed that the loaded concrete specimens (B40-II and B40-III)
31 are more likely to spall than unloaded specimens, with increasing amounts of spalling for higher
32 values of applied load (uniaxial and biaxial loads). Interestingly, it was found that the fire
33 spalling behavior of concrete slabs in unloaded conditions (0 MPa) and under a very low biaxial
34 load (0.5 MPa, parallel to the heated face of the slab) can present two different scenarios. In the
35 first case, no spalling has been observed in the unloaded specimen. In the second one, a uniform
36 erosion extended to the whole heated area has been observed, for an average spalling depth of
37 12 mm. These results demonstrated that very low biaxial compressive loading can influence the
38 fire spalling behavior of concrete, even though 0.5 MPa stress is very small compared to the
39 compressive strength of concrete (51 MPa at the day of the fire test). This higher spalling
40 behavior could not be explained only by the higher stresses (induced by the higher external
41 load) but also by the higher pore pressure induced by a lower damage state and permeability
42 (Felicetti and Lo Monte [4] and Choinska et al. [5]). Felicetti and Lo Monte [4], by
43 implementing on the same biaxial fire tests an innovative technique based on ultrasonic pulse-
44 echo have shown that damage was significantly reduced when the slabs were loaded, even at a
45 very low biaxial stress (e.g. 0.5 MPa). Limited biaxial loads then can affect in a non-negligible

46 way the thermally induced microcracking and then reduce concrete permeability at high
47 temperature.

48 Choinska et al. [5] showed that the permeability of concrete during heating up to 150 °C
49 under uniaxial compressive loading (stress levels lower than 80% of the peak stress) is smaller
50 than the permeability measured after unloading. Lion et al. [6] reported that the apparent
51 permeability, measured after cooling, was lower when confining pressure was increased from 4
52 to 28 MPa and this was more significant for the higher thermal load. Chen et al. [7] tested the
53 gas permeability of heat-treated mortars at four different levels of confining stresses (5, 12, 15
54 and 25 MPa). The authors observed that the permeability of mortars heat-treated above 400 °C
55 was sensitive to confining pressure and the intrinsic permeability decreased by up to 23% when
56 the confining stress increased from 5 to 25 MPa. Pei et al. [8] carried out longitudinal
57 permeability and porosity tests on normalized mortar under different levels of confining
58 pressure (5, 10, 20, 30 and 40 MPa). Their results showed that permeability decreases with the
59 increase of confining pressure and shows a greater sensitivity to confining pressure at higher
60 temperatures due to the closure of the cracks.

61 In order to gain a deeper understanding of the role of heating and loading on the permeability
62 of concrete and to provide more insight into the mechanism behind the fire spalling of concrete,
63 two ordinary concretes were tested. Residual longitudinal and radial permeability tests were
64 carried out in unloaded and loaded (i.e. confining pressure and uniaxial compressive load)
65 conditions on specimens. For an in-depth knowledge of the relationship between permeability
66 and fire spalling, the permeability tests were conducted on the same two concrete mixes (B40-II
67 and B40-III: $f_{c28days} \approx 40$ MPa) that have been studied in Miah et al. [3]. A more detail fire
68 behavior of these two concretes (B40-II and B40-III) such as fire spalling, thermal properties,

69 mechanical properties, porosity, water absorption capacity and permeability in unloaded
 70 condition were investigated in Miah [9], Mindeguia [10], Carré et al. [11] and Mindeguia et al.
 71 [12-14].

72

73 **2 Experimental investigations**

74 2.1 Materials and concrete mix design

75 Two ordinary concretes, B40-II and B40-III, made respectively, with CEM II (CEM II/A-LL
 76 42.5 R CE CP2 NF) and CEM III (CEM III/A 42.5 N CE CP1 NF) cements (NF EN 197-1:2012
 77 [15]) have been investigated. The same mix design was used for both concretes; the only
 78 difference is the cement type. The CEM II cement contains 85% of clinker, 12% of calcareous
 79 fillers and 3% of slag, while the CEM III cement contains 54% of clinker, 3% of calcareous
 80 fillers and 43% of slag. The compressive strength (f_c) and splitting tensile strength (f_t) of both
 81 concretes were conducted according to NF EN 12390-3:2012 [16] and NF EN 12390-6:2012
 82 [17], respectively, on cylindrical samples (diameter = 150 mm and height = 300 mm) at the age
 83 of 28 and 90 days. Constituents and concrete properties at the fresh and hardened state are
 84 reported in Table 1.

85 Table 1. Concrete mixture proportions and properties of hardened concrete

B40 Concrete	Unity	B40-II	B40-III
CEM II/A-LL 42.5 R CE CP2 NF (C)	kg/m ³	350	
CEM III/A 42.5 N CE CP1 NF (C)	kg/m ³		350
Calcareous 8/12.5 gravel	kg/m ³		330
Calcareous 12.5/20 gravel	kg/m ³		720
0/2 siliceous sand	kg/m ³		845
Water (W)	l/m ³		189
Water / cement ratio (w/c)			0.54
28 days compressive strength	MPa	41.1 (36.4 – 46.8)	41.0 (36.1 – 46.5)
90 days compressive strength	MPa	50.9 (49.0 – 52.3)	50.4 (47.8 – 55.3)
28 days tensile strength	MPa	3.9 (3.9 – 4.0)	3.8 (3.7 – 3.9)
90 days tensile strength	MPa	4.8 (4.1 – 5.5)	4.3 (4.0 – 4.7)

86

87 2.2 Experimental programs, apparatus, and test procedures

88 2.2.1 Experimental program

89 Three different gas permeability tests were carried out in SIAME and CSTB. Within the scope
90 of the study, a total of 40 concrete disc specimens were tested and about 200 measurements were
91 carried out, see Table 2.

92 Table 2. Summary of the experimental test program.

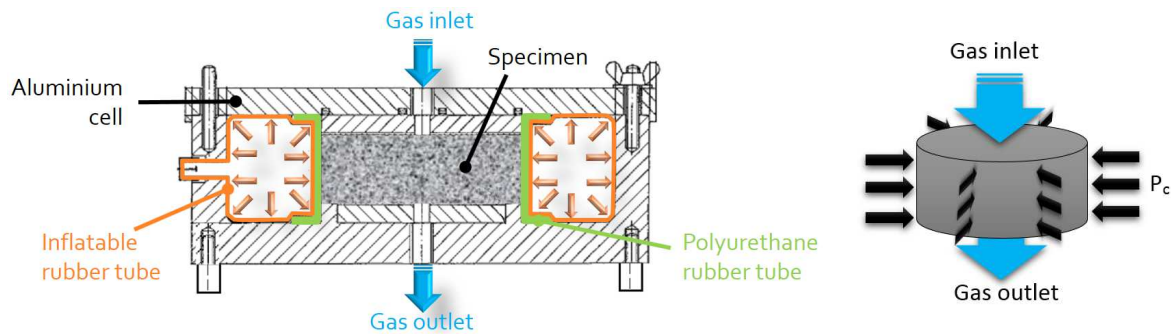
T [°C]	80	120	250	400	600	800
i) Axial permeability tests under radial confining pressure ($P_c = 0.3, 0.6, 0.9$ and 1.2 MPa) after unloaded preheating	2/2	2/2	2/2	2/2	2/2	2/2
ii) Axial permeability tests under P_c of 0.6 MPa after preheating under uniaxial loading ($\sigma = 0, 0.5, 1.5, 3$ and 5 MPa)	–	–	–	2/2	–	–
iii) Radial permeability tests under uniaxial loading ($\sigma = 0.6, 0.9, 1.2, 2, 3, 5$ and 10 MPa) after unloaded preheating	–	2/2	2/1	2/2	1/–	–

93 **Note: X/Y denotes the number of tested specimens (X B40-II samples and Y B40-III samples).**

94

95 2.2.2 Axial permeability tests under radial confining pressure after unloaded preheating

96 The residual axial gas permeability of concrete was measured on 150 mm diameter and 50 mm
97 thickness concrete disc (Fig. 1 right) using a Cembureau constant pressure permeameter (Fig. 1
98 left) (Kollek [18]). The concrete discs were cut from cylindrical specimens of 150 mm diameter
99 and 300 mm height using a diamond disc. Upper and lower discs were not used to avoid the edge
100 effect which could influence the measurements of permeability. The curved side of the specimen
101 was wrapped with aluminum foil tape to ensure a good seal and to prevent leakage of gas
102 through the curved side of the specimen in order that the flow occurs uniaxially through the
103 thickness of the specimen.



104 Fig. 1. Details of the permeability cell (left) (Kollek [18]) and confining pressure (P_c) and axial
 105 gas flow (right).

106 The permeability of concrete was investigated at room temperature after applying thermal
 107 loads of 120, 250, 400, 600 and 800 °C at a slow heating rate of 1 °C/min. The slow heating rate
 108 of 1 °C/min was chosen to limit undesirable thermal stress. After reaching the target temperature,
 109 the temperature was stabilized for 28, 10, 6, 6 and 6 hours, respectively, for the temperatures of
 110 120, 250, 400, 600 and 800 °C (Hager [19]) to reach a uniform temperature in the concrete. The
 111 specimens were then cooled down to room temperature at a rate of lower than 1 °C/min inside the
 112 closed furnace. The reference specimens were dried in an oven at the temperature of 80 °C until a
 113 constant value of mass was reached (around 2 months) to evaluate water content.

114 To study the effect of confining pressure (perpendicular to the gas flow, Fig. 1 right) on the gas
 115 permeability of concretes (B40-II and 40-III), four different levels of radial confining pressure (P_c
 116 = 0.3, 0.6, 0.9 and 1.2 MPa, see Table 2) have been investigated. This was achieved by increasing
 117 the inflatable rubber tube pressure applied to the polyurethane rubber ring (Fig. 1 left). To ensure
 118 that the lowest applied load (0.3 MPa) is sufficient to prevent leakage of gas through the curved
 119 side, blank tests on an aluminum disc of the same dimensions (150 mm diameter and 50 mm
 120 thickness) were performed at 0.3 and 0.6 MPa. No outflow occurred at these lower confining
 121 pressures. Therefore, these blank tests demonstrated that the permeability test results of the

122 concrete specimens were not affected by leakage through the curved side even when applying the
123 lower load value.

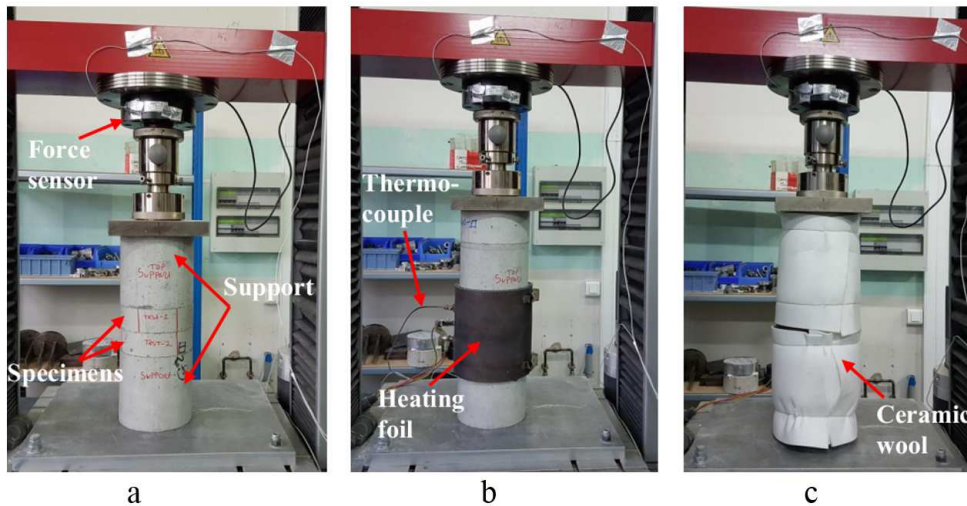
124 Nitrogen has been chosen as the neutral percolating gas. Three levels of pressure difference
125 ΔP (the difference between the injection pressure P_{inj} and the atmospheric pressure P_{atm}) were
126 chosen depending on preheating temperatures in order to determine the intrinsic permeability of
127 concretes according to the Klinkenberg's approach (Klinkenberg [20]). Inlet pressures were
128 applied and maintained until gas flow stabilization.

129

130 2.2.3 Axial permeability tests under radial P_c of 0.6 MPa after preheating under uniaxial loading

131 The test method was similar to the test method described in previous section 2.2.2. The
132 difference was that the specimens were preheated under a constant uniaxial compressive loading
133 (Fig. 2). The size of the specimens was same as described in section 2.2.2. Only one heating
134 temperature (400 °C) was studied and the permeability tests were performed with one confining
135 pressure ($P_c = 0.6$ MPa). Prior to heating, all the specimens, as well as both concrete supports,
136 were ground in order to obtain two faces (upper and lower faces) parallel and plane to ensure a
137 uniform stress distribution in the specimens. Before heating, the specimens were wrapped by
138 means of a heating blanket (Fig. 2b) and a thermal insulator made with ceramic wool (Fig. 2c)
139 and was placed between both concrete supports in the compression testing machine. The
140 specimens were slowly heated (heating rate = 1 °C/min), stabilized for 8 hours, and then cooled
141 down to ambient temperature inside the heating device. The thermal insulator (i.e. ceramic wool)
142 ensure an appropriate increase of temperature during heating the specimens. Before heating, a
143 constant uniaxial compressive load was applied and then maintained constant during the heating
144 process, stabilization and cooling phases. Five different levels of uniaxial compressive stresses

145 (0, 0.5, 1.5, 3 and 5 MPa) have been investigated on both concretes (B40-II and B40-III), see
146 Table 2.



147 a b c
148 Fig. 2. Sample preparation before preheating under uniaxial loading of the test specimens (a.
149 specimen and concrete supports – b. specimen wrapped in the heating blanket – c. specimen with
150 insulating wool).

151 2.2.4 Radial permeability tests under uniaxial loading after heating without any applied preload

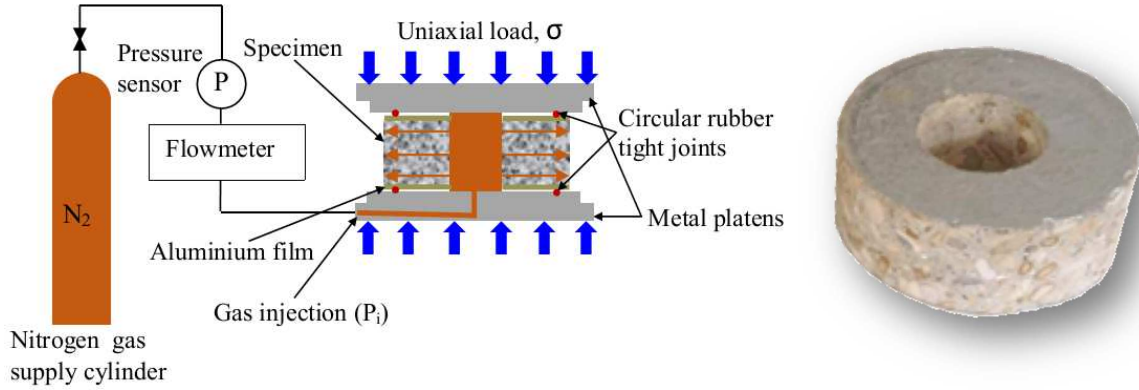
152 The principle of this test was to measure the radial permeability by injecting the nitrogen gas
153 inside a hollow concrete cylindrical disc and then measure the radial gas flow of the specimen
154 (Fig. 3). The hollow discs had external diameter, internal diameter and thickness equal to 123, 52
155 and 50 mm, respectively (Fig. 3 right). The concrete hollow discs were cut from cylindrical
156 specimens of 150 mm diameter and 300 mm height using a diamond blade and, as in the
157 previously described test, ground in order to obtain two faces (upper and lower faces) parallel
158 and plane to ensure a uniform stress distribution in the specimens. The specimens were drilled in
159 order to obtain 123 mm in outer diameter as well as to have better gas transfer, by avoiding the
160 edge effect, through the radial sides during the permeability test. The inner diameter is 52 mm

161 and the thickness 50 mm. The top and bottom faces of the specimens were sealed with aluminum
162 foil tape to prevent leakage of gas along the interface (Fig. 3 right). The heating rate and the
163 temperature levels were same as described in section 2.2.2.

164 In a similar way than the 2 methods described before, a constant relative pressure of the gas ΔP
165 (the difference between the absolute injected pressure P_i and atmospheric pressure P_{atm}) is applied
166 until the gas flow through the material is stabilized (permanent regime). The sample is placed in
167 the permeameter cell between two metal plates (Fig. 3). The bottom plate is perforated in order to
168 allow injecting the nitrogen at the bottom surface of the sample at a pressure P_i . The diameter of
169 the plates is adapted for centering the cylindrical specimen. The nitrogen pressure is regulated by
170 means of a controller and measured with the pressure sensor. In order to ensure a radial gas flow
171 through the specimen, a circular rubber (Fig. 3 left) seals the connection between the specimen
172 and the press plates. A minimal load (0.6 MPa) was applied on the specimen to maintain the good
173 contact between the metal plates and the specimen faces by pressing the circular rubber joints.

174 In this device, the flow rate is measured upstream of the specimen by a mass flow meter, that
175 converts a mass flow into a normalized volume flow. Flow and pressure measurements can be
176 monitored in real time to control flow stabilization. In this testing setup, a time between 10 and 15
177 minutes is required for the gas flow to reach steady state conditions. Through flow measurement,
178 the intrinsic permeability is determined by the Klinkenberg method (Klinkenberg [20]).

179



180 Fig. 3. Schematic diagram of the radial permeability test under uniaxial loading device (left) and
 181 sample geometry (right).

182 The radial permeability measurements are carried out as part of a radial flow of the gas in
 183 steady state. The apparent permeability of a specimen is determined from Darcy's law applied to
 184 a laminar flow of a compressible fluid (gas). Thus, the apparent permeability K_a [m^2], based on a
 185 measurement of the upstream volumetric flow rate Q_i [m^3/s] at injection pressure P_i (Pa), is
 186 given by the following relationship (Choinska et al. [5]):

$$187 \quad K_a = \frac{Q_i P_i \mu \ln\left(\frac{r_2}{r_1}\right)}{\pi h (P_i^2 - P_{atm}^2)} \quad (1)$$

188 where: μ [Pa.s] is the dynamic viscosity of the inlet gas used (nitrogen), P_{atm} [Pa] is the
 189 atmospheric pressure; r_1 [m], r_2 [m], h [m] are the inner radius, outer radius, and height of the
 190 cylindrical specimen respectively.

191 Before the test, a **minimal** compressive stress of 0.6 MPa was applied. This low load ensures
 192 the tightness of the permeability cell and then leads only to a radial gas flow. The value
 193 determined under the lower value of 0.6 MPa (equal to the preload compression stress) is assumed
 194 to be the reference permeability for this test. To study the effect of uniaxial compressive loading

195 on the radial gas permeability of concrete, seven different levels of compressive loading (0.6, 0.9,
 196 1.2, 2, 3, 5 and 10 MPa, Table 2) have been investigated on both concretes.

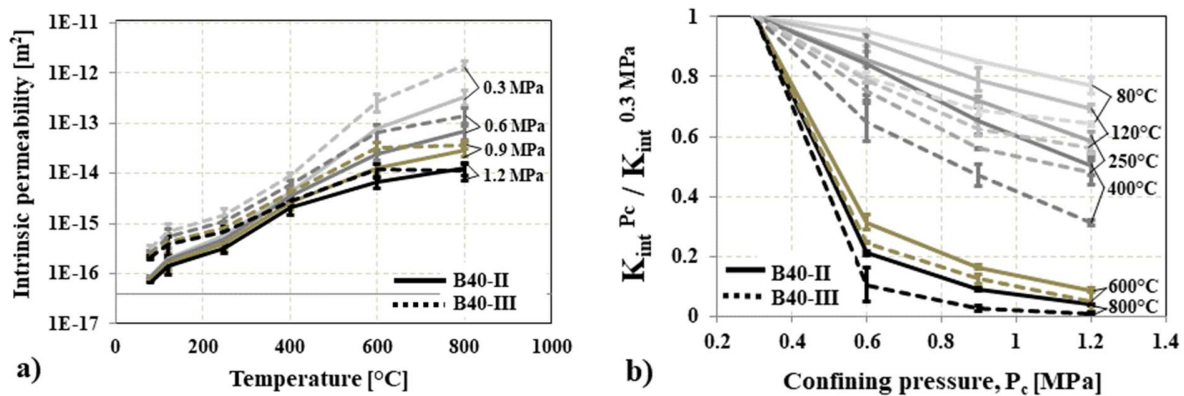
197

198 **3 Experimental results and discussion**

199 3.1 Effect of radial confining pressure on the residual axial gas permeability of concrete

200 The residual axial intrinsic permeability (K_{int}) of concrete specimens subjected to different
 201 preheating temperatures at different levels of radial confining pressure (P_c) is shown in Fig. 4a.

202 For an in-depth analysis of the influence of radial confining pressure on the axial permeability, it
 203 is worthwhile to study the variation in permeability, normalized with respect to the reference
 204 value of confining pressure, i.e. $K_{int}(P_c)/K_{int}(P_c = 0.3 \text{ MPa})$ (Fig. 4b). In Fig. 4, the lines
 205 represent the average value and the vertical line represents the range of data.



206 Fig. 4. Axial intrinsic permeability of concretes under different levels of confining pressure as a
 207 function of temperature (a) and normalized permeability versus radial confining pressure (b).

208 In Fig. 4a, it can be seen that as the temperature increased, the permeability increased with
 209 higher increments at the higher temperatures (note that the figure is in logarithmic scale for the
 210 permeability). Between 80 °C and 120 °C, rather sharp increase of axial permeability was
 211 observed for both concretes. This behavior was observed by Kalifa et al. [21] in the temperature

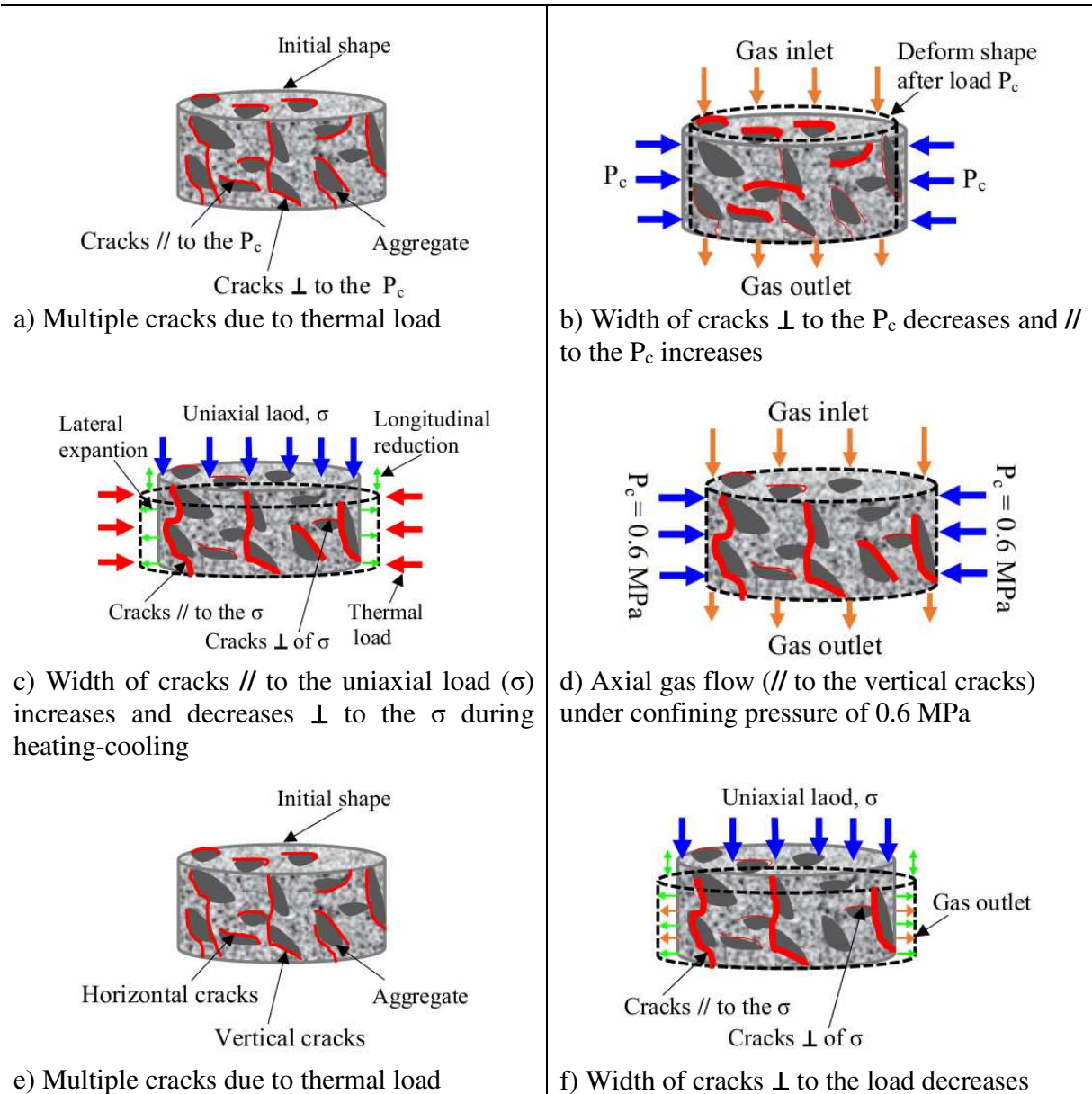
212 range between 80 °C and 105 °C. This behavior could be due to accessible pore volume caused
213 by the removal of the free water and the physically bound water that was not withdrawn at 80 °C.
214 Above 400 °C, the increase of the permeability may be attributed to the development of cracks
215 mainly caused by the thermal incompatibility between the cement paste and the aggregates
216 (Kalifa et al. [21]), since at high temperature the cement paste shrinks due to dehydration, while
217 the aggregates dilate due to their thermal expansion. This mismatch induces tensile stresses in
218 the matrix and compressive stresses in the aggregates which in turn can lead to cracks formation.
219 In Fig. 4b, the experimental results showed that the axial permeability of 2 concretes (B40-II and
220 B40-III) decreased with increasing radial confining pressure (P_c perpendicular to the gas flow,
221 Fig. 1 right). It can be seen that the residual permeability after preheating at 80 °C and 120 °C
222 are hardly sensitive to confining pressure. This can be explained by the lower amount of
223 microcracks and cracks induced by the lower preheating temperatures. On the contrary, these
224 effects are more pronounced when the preheating temperatures are higher (e.g. at 600 °C and 800
225 °C). It is important to notice that, as previously mentioned, the decreased trend of permeability
226 with increasing radial confining pressure is not due to leakage of gas, since no outflow occurred
227 at confining pressure starting from 0.3 MPa during the blank test. This behavior should be
228 attributed to the partial closure of heat induced microcracks and cracks (parallel to the gas flow)
229 located at the aggregate-cement paste interface and through the aggregates. Indeed, the cracks
230 perpendicular to the applied compressive stress (here stress due to confining pressure) close (Pei
231 et al. [8]) while those parallel to the compressive stress tend to open (Mindeguia et al. [22],
232 Huismann et al. [23] and Ring et al. [24]) (Fig. 5a and 5b). Fig. 5 is a schematic diagram
233 showing the crack width changes with the effect of temperature and mechanical loading.
234 Though, no measurement of crack openings were carried out on the tested samples, the

235 development of cracks presented in Fig. 5 is in good agreement with the permeability
 236 measurements and the results presented in Choinska et al. [5]. Crack width changes with
 237 temperature depend on concrete mixes and can be largely dependent on the nature of
 238 aggregates. As an example, crack widths of concretes containing flint aggregates are larger than
 239 most of other concretes when exposed to temperatures higher than 300 °C (Hager [19]). From
 240 the literature, it can be shown that the crack width of concretes heated at 300 °C and 400 °C can
 241 be about 3 µm (Huismann et al. [23]) and 10 µm (Kalifa et al. [21]), respectively. While Chen et
 242 al. [7] observed that the crack width of mortars heated at 400 °C can be about 2 to 5 µm.

243 Interestingly, a sharp decrease of permeability can be seen when the confining pressure was
 244 doubled ($P_c = 0.6$ MPa) than the reference pressure ($P_c = 0.3$ MPa). At the higher temperatures
 245 (600 °C and 800 °C), when the confining pressure continues to increase beyond 0.6 MPa, a lower
 246 decreasing rate of permeability is observed, and the permeability tends to stabilize. Fig. 4b
 247 suggests that, when temperatures are lower than 600°C, the crack closure and the decrease in
 248 permeability could continue if the confinement would have been increased beyond 1.2 MPa
 249 (which was the limitation of the test device). The presented results are in good agreement with
 250 the results reported in the literature even though most of the studies have been carried out at
 251 confining pressures that are much higher than in our tests (Lion et al. [6], Chen et al. [7] and Pei
 252 et al. [8]).

253 Fig. 4 allows us to compare the axial gas permeability of B40-II (3% of slag) and B40-III
 254 (43% of slag). It can be observed that the permeability of B40-III is higher for all the
 255 temperatures under 0.3 MPa confining pressure. The permeability difference between 2
 256 concretes decreases when confining pressure increases.

Before permeability tests (i.e. during heating)	During permeability tests
---	---------------------------



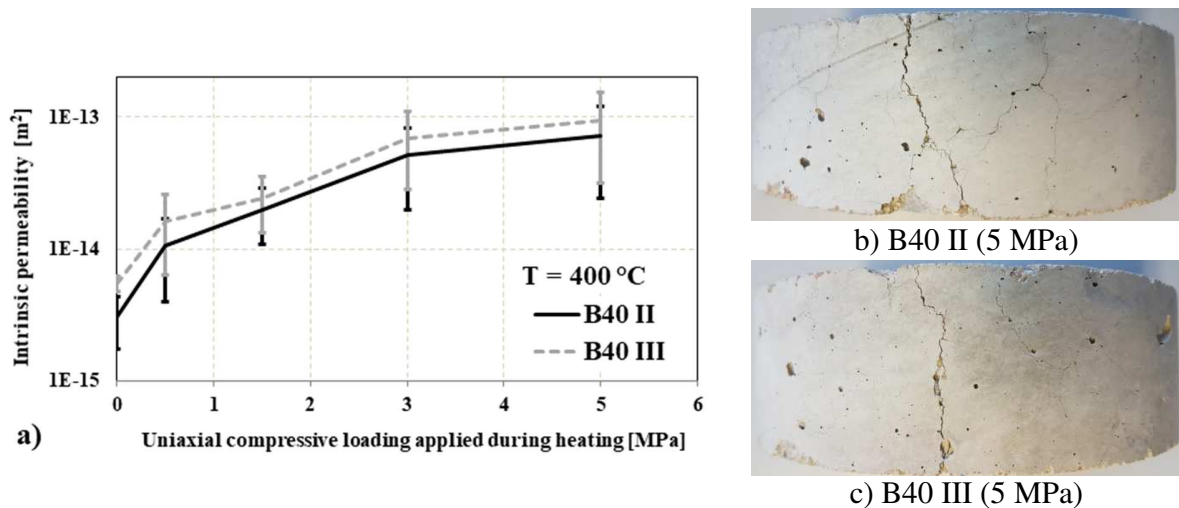
257 Fig. 5: Schematic diagram of the crack patterns and their effect on heating and different loading
 258 conditions (Note: \perp = perpendicular, \parallel = parallel).

259 3.2 The effect of uniaxial loading during heating-cooling on the axial gas permeability of concrete

260 The residual axial intrinsic permeability of the B40-II and B40-III concrete specimens
 261 subjected to preheating (400 °C) under different levels of uniaxial compressive loading is
 262 presented in Fig. 6a. In the **diagram**, the lines represent the average value and the vertical line

263 represents the range of data. In this experimental test campaign, an increasing trend of intrinsic
 264 axial gas permeability was observed with the increased uniaxial compressive loading (parallel to
 265 the gas flow) applied during the heating-cooling phases. Interestingly, a higher increase of
 266 intrinsic axial gas permeability was observed in the specimens which were loaded at low
 267 compressive loading (0.5 MPa). **These results show that** very small compressive loading can
 268 influence the axial gas permeability of concrete, even though 0.5 MPa stress is very small
 269 compared to the compressive (f_c) strength of concrete ($f_c \approx 50$ MPa at the day of the tests, see
 270 Table 1). **It is to be noted that the heating of the specimens were carried out at 90 days. This age**
 271 **was chosen because at 28 days, the hydration of blended cements, as cements containing slags, is**
 272 **not completed and because 90 days is the advised age for laboratory tests in order to study a**
 273 **stabilized concrete with regard to its main properties (e.g. compressive strength).**

274



275 Fig. 6. Residual axial permeability measured after preheating under different levels of uniaxial
 276 compressive loading (a) and image of cracks parallel to the loading direction ($\sigma = 5$ MPa) (b-c).

277 When concrete is heated under a constant uniaxial compressive loading, its longitudinal strain
 278 is reduced. This reduction is mostly induced by transient thermal strain (Mindeguia et al. [22]).

279 By opposite, radial strains tend to be higher. This is mainly explained by the formation and
280 opening of cracks parallel to the loading direction (Mindeguia et al. [22], Huismann et al. [23]
281 and Ring et al. [24]) (see Fig. 5c). The evidence of cracks parallel to the loading direction after
282 heat treatment at 400 °C under uniaxial loading (5 MPa) can be clearly seen in Fig. 6b and 6c.
283 No similar cracking was observed in the unloaded specimens. These axial cracks explain the
284 higher axial gas permeability measured in these tests, since the injected gas flow was along the
285 compressive loading direction (Fig. 5d).

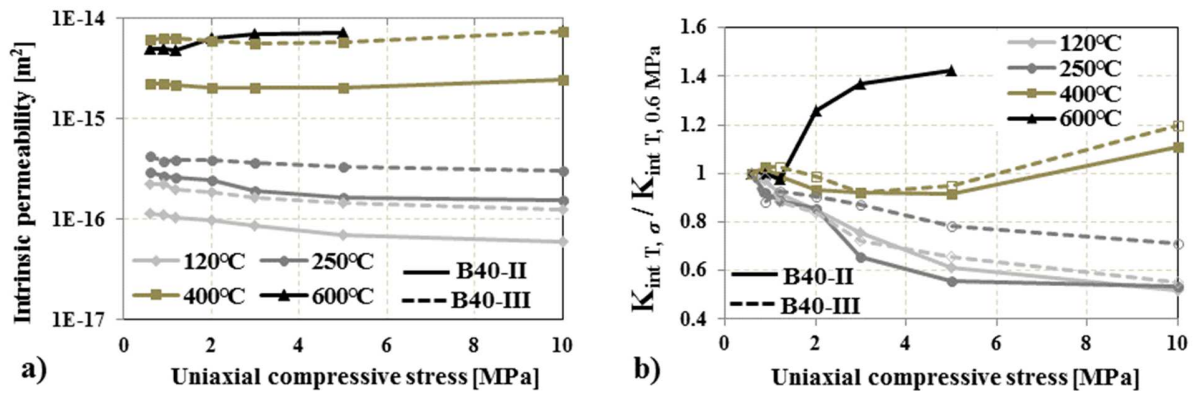
286 An important observation from Fig. 6a is that the residual axial permeability of B40-III (43%
287 of slag) is higher than B40-II (3% of slag) in all the temperatures, which is in good agreement
288 with the former tests that have presented in section 3.1 and Miah et al. [25].

289 3.3 The effect of uniaxial loading on the residual radial gas permeability of concrete

290 Fig. 7a presents the residual radial intrinsic permeability (K_{int}) of concretes (B40-II and B40-
291 III) **depending on** uniaxial compressive stress. The relationships between the normalized
292 permeability and the uniaxial compressive stress are shown in Fig. 7b. It can be seen that in Fig.
293 7b, at lower temperatures (120 °C and 250 °C), permeability decreases when applied
294 compressive stress increases, **while at higher temperatures (400 °C and 600 °C)**, the permeability
295 decreases up to a certain level of load, after that stabilizes and then increases when the
296 compressive stress increases.

297 In general, the trend presented in Fig. 7b clearly indicates distinct phases in the variation in
298 radial permeability with the load. First, permeability decreased with the increasing applied
299 compressive loading (for all temperature levels). This phenomenon is attributed to the partial
300 closure of heat-induced microcracks and cracks (perpendicular to the load) caused by the
301 increase in the applied compressive loading (Fig. 5f). It appears between 0.6 and 5 MPa for the

302 heating at 120 °C and 250 °C, between 0.6 and 2 MPa for 400 °C and between 0.6 and 0.9 for
 303 600 °C.



304 Fig. 7. Effect of uniaxial compressive loading on the radial gas permeability of concretes.

305 Secondly, a very small change or even almost constant permeability was observed. The
 306 observation in this phase can be explained by the counterbalancing of the cracks initiation and
 307 cracks growth by the cracks closure. This phase is observable up to 5 MPa for 120 °C and 250
 308 °C, between 2 and 5 MPa for 400 °C and between 0.9 and 1.2 MPa for 600 °C.

309 Finally, an increase in permeability was observed with the further increase of the
 310 compressive stress. At 120 °C and 250 °C, the applied stress (10 MPa) is not sufficient to
 311 observe increase of permeability due to additional mechanical damage. For B40-II specimens
 312 heated at 400 and 600 °C, the phenomenon is observed above 5 and 1.2 MPa, respectively (Fig.
 313 7b). Almost similar behavior was found for the B40-III preheated at 400 °C; The specimens
 314 preheated at 600 °C were more damaged during heating. Hence, it was not possible to measure
 315 the permeability due to the very fast gas flow.

316 The increasing permeability with increasing loads could be due to the extension of the
 317 existing cracks, creation, and opening of new cracks (Bian et al. [26]) due to Poisson's effect
 318 (i.e. increase transversal deformation due to crack opening in the direction of the gas flow).

319 As we have seen in sections 3.1-3.2 and in Miah et al. [25], B40-II (3% of slag) always
320 exhibited lower permeability than B40-III (43% of slag) in all the heating levels (Fig. 7a). We
321 then observe a good agreement among all the tests.

322

323 **4 Concluding remarks**

324 Permeability of concrete is one of the key parameters controlling internal fluid transfer; **It**
325 **influences the magnitude of pore pressure within the concrete structure which in turn contribute**
326 **to the risk of fire spalling.** It is worth noting, however, **that the many studies** have been
327 conducted on the permeability of concrete at high temperatures under unloaded condition, while
328 comparatively, there are few published data on the permeability of concrete subjected to heating
329 and mechanical loading or under confining condition. To this end, axial and radial gas
330 permeability tests were carried out on two ordinary concretes (B40-II and B40-III: $f_{c28days} \approx 40$
331 MPa) under different preheating and loading conditions. **The permeability of concrete was**
332 **investigated at room temperature after applying thermal loads of 80, 120, 250, 400, 600 and 800**
333 **°C at a slow heating rate of 1 °C/min.**

334 The main findings regarding the influence of heating levels, loading type and levels, and
335 cement type on the gas permeability of ordinary concrete can be summarized as follows:

- 336 I. **As temperature increases, gas permeability increases as well, and the higher the**
337 **temperature, the higher the increment.**
- 338 II. **The residual axial permeability of concretes (B40-II and B40-III) after unloaded**
339 **preheating decreases with increasing radial confining pressure due to partial closure of**
340 **heat induced axial microcracks and cracks (parallel to the gas flow) located at the**
341 **aggregate-cement paste interface and through the aggregates.**

- 342 III. Compressive loading affects concrete residual axial permeability even at low stress levels
343 (i.e. 0.6 MPa) compared with concrete strength ($f_c \approx 50$ MPa at the day of the tests) in
344 compression.
- 345 IV. When specimens are heated under a given preloading, the residual axial gas permeability
346 of concrete increases with the increasing uniaxial compressive loading (parallel to the gas
347 flow) applied during the heating-cooling phases. This behavior should be attributed to the
348 formation and opening of cracks parallel to the direction of the compressive loading
349 applied during preheating.
- 350 V. At lower temperatures (120 °C and 250 °C), the radial residual permeability under
351 uniaxial loading after heating without any applied preloading decreases with increasing
352 uniaxial compressive stress. While at higher temperatures (400 °C and 600 °C), the radial
353 permeability decreases up to a certain level of load, after that stabilizes, and then
354 increases when the uniaxial compressive stress increases. Such behavior may be
355 explained by the combination of two competing effects, crack closing due to compressive
356 stresses and crack opening due to the lateral expansion (Poisson's effect).
- 357 VI. Concrete permeability increases or decreases depending on the loading conditions and
358 becomes anisotropic. Hence, the stress state, by governing the orientation and opening of
359 the cracks is a key factor in controlling the transport of internal fluids (i.e. permeability)
360 and then directly triggers the build-up and magnitude of the pore pressure within the
361 concrete structure. Stress state has then 2 major roles on concrete fire spalling: (1) a
362 direct influence in the thermo-mechanical mechanism and (2) an indirect influence in
363 thermo-hydral mechanism by influencing the cracks opening and orientation and then, the
364 permeability.

365 VII. The permeability of B40-III (43% of slag) is higher than B40-II (3% slag) in all heating
366 and loading conditions. Even if pore pressure is not the only driving force of spalling,
367 these results (i.e. lower pore pressure due to higher permeability of B40-III at high
368 temperatures) tends to show that the studied B40-III concrete could be less sensitive to
369 fire spalling than B40-II concrete.

370

371 **Acknowledgements:**

372 This research was carried out in the frame of a large collaboration, on the influence of the
373 mechanical loading on concrete spalling, between three laboratories: Politecnico di Milano,
374 SIAME, and CSTB. Authors would like to thank Roberto Felicetti and Francesco Lo Monte of
375 the Politecnico di Milano for the fruitful discussion.

376

377 **Funding:** This research did not receive any specific grant from funding agencies in the public,
378 commercial, or not-for-profit sectors.

379

380 **References:**

381 [1] V.V. Zhukov, Reasons of explosive spalling of concrete by fire, Beton i zhlezobeton
382 (Concrete and Reinforcement Concrete), Issue 3, 1976.

383 [2] G.A. Khoury, Y. Anderberg, Concrete spalling review, Fire safety design, report submitted to
384 the Swedish National Road Administration, Sweden, 2000.

385 [3] M.J. Miah, F. Lo Monte, R. Felicetti, H. Carré, P. Pimienta, C. La Borderie, Fire Spalling
386 Behaviour of Concrete: Role of mechanical loading (uniaxial and biaxial) and cement type, **Key**

387 Engineering Materials 2016, Vol. 711, pp. 549-555.
388 DOI: [10.4028/www.scientific.net/KEM.711.549](https://doi.org/10.4028/www.scientific.net/KEM.711.549).

389 [4] R. Felicetti, F. Lo Monte, Pulse-echo monitoring of concrete damage and spalling during fire,
390 Proceedings of the 9th International Conference on Structures in Fire, June 8-10, 2016, Princeton,
391 USA.

392 [5] M. Choinska, A. Khelidj, G. Chatzigeorgiou, G. Pijaudier-Cabot, Effects and interactions of
393 temperature and stress-level related damage on permeability of concrete, Cement and Concrete
394 Research 37 (2007) 79–88.

395 [6] M. Lion, F. Skoczylas, Z. Lafhaj, M. Sersar, Experimental study on a mortar. Temperature
396 effects on porosity and permeability. Residual properties or direct measurements under
397 temperature, Cement and Concrete Research 35 (2005) 1937 – 1942.

398 [7] X-t. Chen, G. Caratini, C.A. Davy, D. Troadec, F. Skoczylas, Coupled transport and pro-
399 mechanical properties of a heat-treated mortar under confinement, Cement and Concrete
400 Research 49 (2013) 10–20.

401 [8] Y. Pei, F. Agostini, F. Skoczylas, The effects of high temperature heating on the gas
402 permeability and porosity of a cementitious material, Cement and Concrete Research 95 (2017)
403 141–151.

404 [9] M.J. Miah, The effect of compressive loading and cement type on the fire spalling behaviour
405 of concrete, PhD Thesis, 2017, Université de Pau et des Pays de l’Adour, France.

406 [10] J-C. Mindeguia, Contribution Expérimental a la Compréhension des risqué d’Instabilité
407 Thermiques des Béton, PhD Thesis (French), 2009, Université de Pau et des Pays de l’Adour,
408 France.

- 409 [11] H. Carré, C. Perlot, A. Daoud, M.J. Miah, B. Aidi, Durability of ordinary concrete after
410 heating at high temperature, *Key Engineering Materials* 2016, Vol. 711, pp. 428-435,
411 DOI: 10.4028/www.scientific.net/KEM.711.428.
- 412 [12] J-C. Mindeguia, P. Pimienta, H. Carré, C. La Borderie, On the influence of aggregate nature
413 on concrete behaviour at high temperatura, *European Journal of Environmental and Civil*
414 *Engineering*, Vol. 16, No. 2, February 2012, pp. 236–253.
- 415 [13] J-C. Mindeguia, P. Pimienta, H. Carré, C. La Borderie, Experimental analysis of concrete
416 spalling due to fire exposure, *European Journal of Environmental and Civil Engineering*, 2013,
417 Vol. 17, No. 6, pp. 453–466.
- 418 [14] J-C. Mindeguia, H. Carré, P. Pimienta, C. La Borderie, Experimental discussion on the
419 mechanisms behind the fire spalling of concrete, *Fire and Materials*, November 2015, Vol. 39,
420 Issue 7, pp. 619–635.
- 421 [15] NF EN 197-1, Cement - Part 1: Composition, specifications and conformity criteria for
422 common cements, April 2012.
- 423 [16] NF EN 12390-3: 2012, Testing hardened concrete - Part 3: Compressive strength of test
424 specimens, April 2012.
- 425 [17] NF EN 12390-6: 2012, Testing hardened concrete - Part 6: Tensile splitting strength of test
426 specimens, April 2012.
- 427 [18] J.J. Kollek, The determination of the permeability of concrete to oxygen by the cembureau
428 method - a recommendation, *Materials and Structures* (1989), 22, pp. 225-230.
- 429 [19] I.G. Hager, Comportement à haute température des bétons à haute performance-évolution
430 des principales propriétés mécaniques, PhD Thesis (French), 5 November 2004, l'Ecole
431 Nationale des Ponts et Chaussées et l'Ecole Polytechnique de Cracovie.

- 432 [20] L.J. Klinkenberg, The permeability of porous media to liquid and gases, American
433 Petroleum Institute, Drilling and Production Practice (1941), pp. 200-213.
- 434 [21] P. Kalifa, G. Chéné, C. Gallé, High-temperature behaviour of HPC with polypropylene
435 fibres: from spalling to microstructure, Cement and Concrete Research 31 (2001) 1487–1499
- 436 [22] J-C. Mindeguia, I. Hager, P. Pimienta, H. Carré, C. La Borderie, Parametrical study of
437 transient thermal strain of ordinary and high performance concrete, Cement and Concrete
438 Research 48 (2013) 40–52.
- 439 [23] S. Huismann, F. Weise, U. Schneider, Influence of the preload on the mechanical properties
440 of high strength concrete at high temperatures, Proceedings of the 1st International Workshop on
441 Concrete Spalling due to Fire Exposure, MFPA Institute, Leipzig, ISBN: 978-3-00-028604-9,
442 September 3–5, 2009, pp. 189–200.
- 443 [24] T. Ring, M. Zeiml, R. Lackner, J. Eberhardsteiner, Experimental investigation of strain
444 behaviour of heated cement paste and concrete, Strain (2013), 49, 249–256.
- 445 [25] M.J. Miah, P. Pimienta, H. Carré, N. Pinoteau, C. La Borderie, Fire spalling of concrete:
446 effect of cement type, Proceedings of the 4th International Workshop on Concrete Spalling due to
447 Fire Exposure, October 8-9, 2015, Leipzig, Germany.
- 448 [26] H. Bian, K. Hannawi, M. Takarli, L. Molez, W. Prince, Effects of thermal damage on
449 physical properties and cracking behavior of ultrahigh-performance fiber-reinforced concrete,
450 Journal of Materials Science, 2016, 51 (22), pp. 10066–10076.